Article:
Yue, J., Guo, W., Liang, S. et al. (6 more authors) (2025) Kinetics, contributions, and pathways of the degradation of artificial sweeteners by primary and secondary radicals during UV/persulfate. Separation and Purification Technology, 362 (1). 131683. ISSN 1383-5866

https://doi.org/10.1016/j.seppur.2025.131683

Kinetics, contributions, and pathways of the degradation of artificial sweeteners by primary and secondary radicals during UV/persulfate

Junhui Yue [a], Wei Guo [a, *], Shengxu Liang [a], Martin R. Tillotson [b], Yuhan Zhu [a], Dongyue Li [a], Linzhu Du [a], Jun Li [a], Xu Zhao [c]

[a] National Engineering Laboratory for Advanced Municipal Wastewater Treatment and Reuse Technology, Beijing University of Technology, Beijing 100124, China

[b] School of Civil Engineering, University of Leeds, Leeds LS2 9JT, United Kingdom

[c] Institute of Blue and Green Development, Shandong University, Weihai 264209, China

[*] Corresponding author.

Wei Guo

E-mail address: gwfybj@bjut.edu.cn

Full postal address: Beijing University of Technology, Pingleyuan 100, Chaoyang, Beijing 100124, China.

Abstract: UV/persulfate (UV/PS) is considered an effective process for the degradation of emerging micropollutants in aquatic media. However, under the influence of complex water matrices such as wastewaters, radicals created during UV/PS will be reduced and transformed, so the chemical process of effectively obtaining the radicals in the system is very important to improving degradation efficiency. Thus, in the study, neotame (NEO, an artificial sweetener), as an emerging contaminant, was selected as the target compound to investigate in terms of its degradation and the role of free radicals in a range of water matrices during the UV/PS process. Based on the low concentration probe method (probe concentration ≤ 0.2 μm, more than 3-fold improvement in radical detection accuracy), kinetic modeling was developed to determine the role of primary (•OH and SO_4•$^-$) and secondary (*e.g.* Cl•, Cl_2•$^-$, CO_3•$^-$, and NO_2•) radicals. Results indicated that UV/PS was effective in decomposing NEO (>93.7%) within 7 min and was mainly attributed to •OH and SO_4•$^-$. Acidic environments promote NEO degradation with a greater contribution from SO_4•$^-$. Natural organic matter inhibited NEO degradation by quenching radicals (especially •OH). The k_{obs} of NEO degradation in the presence of Cl^- remained almost unchanged due to the production of Cl• and Cl_2•$^-$ compensating the depletion of SO_4•$^-$. The presence of HCO_3^- quenched a part of primary radicals, which led to a decrease in k_{obs} of NEO degradation, but CO_3•$^-$ began to play a partial degradation role. In the presence of NO_3^-, UV-activated production of •OH and NO_2• promoted NEO degradation. Based on 39 transformation products obtained, 3 degradation pathways and 7 radical attack ways were proposed for NEO degradation by primary and secondary radicals in the

UV/PS system. This study provides meaningful insight into the role of primary and secondary radicals in NEO degradation using UV/PS systems.

Keywords: UV/persulfate; Secondary radicals; Artificial sweetener; Kinetics; Transformation products

1. Introduction

Artificial sweeteners (ASs) are used as sugar substitutes in a variety of foods, beverages, medications and animal feed [1,2]. However, the World Health Organization (WHO) has recently issued new guidelines noting that ASs not only have no long-term benefits for weight loss, but may also have potentially adverse effects, classifying them as possible carcinogens (IARC Group 2B) [3]. In addition, artificial sweeteners have recently been recognized as high-priority emerging contaminants due to their high frequency of detection and high concentrations in various environments [4]. Among the widely used ASs, neotame (NEO) is a second-generation AS synthesized via aspartame and 3,3-dimethylbutyraldehyde [5]. Compared to first-generation ASs (including acesulfame, sucralose, and aspartame), NEO provides higher sweetness (21–65 times), lower production costs, and greater stability [6]. Due to these commercial advantages, its use in many types of sugar substitution products is becoming more widespread [7]. Similar to first generation ASs, its impact on the environment and human health has attracted widespread attention [8,9]. For example, NEO has been detected at concentrations of 0.007–0.17 μg/L and 0.008–0.49 μg/L in aqueous environments and wastewaters, respectively [10-13]. Relatively high concentrations of NEO have also

been detected in sewage sludge and suspended particulate matter at 2–4 ng/g and 20–51 ng/g, respectively [2,14]. Sustained exposure to NEO has been reported to alter the abundance of gut microbiome, decreasing α-diversity, and modifying metabolic patterns [15,16]. NEO exposure also leads to apoptosis and death of intestinal epithelial cells, and can cause barrier disruption and increased monolayer leak [17]. In addition, NEO interferes with enzymes involved in lipogenesis and catabolism and affects neuromodulation of lipid metabolism [18]. Our recent study showed NEO is difficult to remove using traditional wastewater treatment processes (such as flocculation, sedimentation, and biological treatment) in sewage treatment plants (STPs), which results in continuous emission into receiving waterbodies along with treated effluent, thus posing a potential long-term threat to aquatic ecosystems [14]. More importantly, research on effective degradation and contamination control processes for NEO remains a critical knowledge gap. There is therefore an urgent need to devise efficient treatment methods to supplement or replace traditional processes in STPs for improved degradation of NEO in wastewater.

In recent decades, advanced oxidation processes (AOPs) based on the production of hydroxyl radicals (•OH) and sulfate radicals ($SO_4^{\bullet-}$) have been shown to be highly efficient methods for removing recalcitrant organic pollutants in wastewater [19-22]. Amongst AOPs, $SO_4^{\bullet-}$ based oxidation has received the most attention. Compared with •OH, $SO_4^{\bullet-}$ is particularly effective at reacting with organic compounds, and this has been attributed to its higher redox potential (2.5−3.1 V) and longer half-life (30−40 μs) [23]. $SO_4^{\bullet-}$ can be generated by activation of persulfate (PS) through ultraviolet (UV)

84 irradiation [24], electricity [25], transition metals [26] and carbon materials [27].
85 Amongst these methods, UV (<300 nm) activation of PS is the most favorable since it
86 activates PS more effectively (evidenced by a molar absorption coefficient of 16.6 M^{-1}
87 cm^{-1}), and may be integrated into current wastewater flowsheets without necessitating
88 additional chemicals and dosage systems [22,23]. Moreover, UV/PS has been
89 successfully applied to degradation of recalcitrant organic pollutants in wastewater,
90 such as estrogens [28], pesticides [29], and anti-inflammatory drugs [30]. However, to
91 date, limited information is available regarding the role of UV/PS in AS degradation,
92 particularly concerning new ASs like NEO in wastewater.

93 Generally, •OH and SO_4•$^-$ contribute to the degradation of organic pollutants in
94 aquatic media in UV/PS systems [31]. However, in wastewaters, degradation efficiency
95 of organic pollutants using UV/PS may be affected by water matrix components such
96 as pH, natural organic matter (NOM) and some anions [30]. For example, pH
97 significantly affects free radical composition in UV/PS systems, and subsequently the
98 transformation pathways of organic pollutants. In the case of quaternary amine
99 compound degradation using UV/PS/Cu^{2+}, acidic conditions were found to enhance
100 pollutant degradation, whereas alkaline conditions had an inhibitory effect [32].
101 Detailed investigations revealed a substantial increase (8- to 26-fold) in •OH
102 contribution under alkaline conditions, whereas SO_4•$^-$ played a more dominant role
103 (1.1- to 1.2-fold increase) in acidic environments [32]. NOM and inorganic anions
104 diminish UV flux within the system and quench some radicals, thereby impeding
105 organic pollutant degradation [33]. In addition, •OH and SO_4•$^-$ in UV/PS systems can

106 be converted to secondary radicals (*e.g.*, Cl•, Cl_2^{-}•, CO_3•$^{-}$, and NO_2•) by reacting with
107 inorganic anions including Cl^{-}, HCO_3^{-} and NO_3^{-} [34-36]. These secondary radicals
108 usually have high oxidation potentials (*e.g.*, 2.50 V, 2.20 V, and 1.60 V for Cl•, Cl_2^{-}•,
109 and CO_3•$^{-}$, respectively), which may significantly contribute to the degradation of
110 organic pollutants [37]. Despite acknowledging the significant role of secondary
111 radicals, there remains a shortage of detection tools to measure secondary radical
112 concentrations during UV/PS treatments. Chemical probes are widely used to
113 determine the concentration of radicals in photochemical-AOPs, however the probe
114 method suffers from two drawbacks in most studies. First, the chemical processes of
115 radicals in the system are drastically changed due to high probe concentrations [38].
116 Second, there is a lack of research on multiprobe coupling and detection, which has led
117 to applications only in primary radical quantification [39]. Therefore, there is a need to
118 develop a low concentration coupled probe method to simultaneously monitor primary
119 and secondary radical concentrations, and to assess the specific role of secondary
120 radicals in UV/PS for NEO degradation.

121 Although UV/PS is capable of removing a wide range of organic pollutants, it is
122 difficult to fully mineralize them, thus generating a wide range of transformation
123 products (TPs) [40,41]. TPs have greater polarity due to higher oxidation, such that they
124 are more persistent and mobile in soil and water environments and thus may accumulate
125 [42]. The wide distribution of TPs raises concerns about safety. For example, it has been
126 shown that photo-induced degradation of Acesulfame results in TPs up to 500 times
127 more toxic than the parent compound [43]. Therefore, there is a need to further

characterize the occurrence and toxicity of relevant TPs of NEO. In addition, multiple radicals in the system have different propensities to attack functional groups, and thus may play diverse roles in the induction and toxicity changes of TPs [44]. For example, during the degradation of gemfibrozil using UV/PS/Cl^-, it was found that •OH hydroxylates the benzene ring, and the occurrence of phenolic functional groups may lead to increased toxicity [45]. In contrast, SO_4•$^-$ breaks the ether bond of gemfibrozil and possibly aids in the removal of toxic groups [45]. Consequently, the degradation process does not necessarily reduce the toxicity of the solution, so it is necessary to evaluate the different radical-induced TPs and evaluate the toxicity of the resulting solution.

Thus, the objectives of this study were: (1) to investigate the performance and degradation kinetics of UV/PS for NEO degradation in the aquatic environment; (2) to construct a low concentration coupled probe model in UV/PS for investigating the concentration and role of primary and secondary radicals under actual matrix conditions (including pH, natural organic matter, and inorganic anions); (3) to identify possible generated TPs and degradation pathways of NEO by high-resolution mass spectrometry and density functional theory (DFT); and (4) to evaluate the toxicity risk of TPs in the system through *Vibrio fischeri* acute toxicity testing and computational toxicology. The results can provide helpful information for applicability and mechanistic understanding of AS degradation by UV/PS in real contaminated water.

2. Materials and methods

150 *2.1 Chemicals*

151 All chemicals used in experiments were at least analytical grade, as described in Text
152 S1 of the Supporting Information (SI). A Milli-Q purification system (Millipore Co.,
153 France) was used to prepare deionized water to configure all solutions.

154 *2.2 Experimental procedures*

155 The experimental setup for photochemistry is depicted in Fig. S1. A low-pressure
156 mercury lamp (10 W, 254 nm) with an electronic ballast was positioned at the center of
157 the reactor, providing an irradiation intensity of 18.5 W/m². The experiment involved
158 adding NEO (5 μM) and phosphate buffer (2 mM) to a 50 ml quartz tube reactor. UV
159 irradiation initiated the reaction after introducing 50 μM PS. Magnetic stirring ensured
160 proper mixing of the solution during degradation, and a water circulation cooling
161 system keeping solution temperature at 25 ± 0.2℃. $Na_2S_2O_3$ solution was pre-added to
162 2 mL samples and used as a quencher. At predetermined intervals, 1 mL sample solution
163 was transferred into a sample bottle. The change of pH of the solution before and after
164 the experiment was less than 0.2.

165 Depending on experimental design, the pH value was adjusted within the range 6 -
166 8. Additionally, specific concentrations of humic acid (HA; used as a model compound
167 for natural organic matter, at 1 and 5 mg C/L), Cl^- (at 1 and 5 mM), HCO_3^- (at 1 and 5
168 mM), and NO_3^- (at 1 and 5 mM) were introduced into the system for kinetic analysis.
169 $HClO_4$ and NaOH were used to adjust the initial pH of the reaction solution. The
170 presence of $HClO_4$ does not affect the removal of NEO (Fig. S2).

171 Radical identification was performed by quenching experiments (tert-butanol and

methanol) and electron paramagnetic resonance (EPR) experiments, which showed that the primary radicals were •OH and SO_4•$^-$ (Text S14 for related identification analysis) [32]. Then, low concentration probe models were constructed by adding probes in pure water or water matrix systems. Bezafibrate (BZF) and p-chlorobenzoic acid (pCBA) were used as probe compounds added simultaneously to the UV/PS system to determine the concentrations of •OH and SO_4•$^-$. The impact of probe concentration on radicals was explored by varying the amount of probe added (0.05−2.0 μM), and then the optimum probe concentration (0.1 μM) was determined. In the UV/PS/Cl^- system, 0.1 μM pCBA, 0.1μM BZF, 0.1μM 2,4,6-trimethylbenzoic acid (TMBA), and 0.2 μM naproxen (NPX) were added simultaneously as probe compounds for •OH, SO_4•$^-$, Cl•, and $Cl_2$$^-$•. For the UV/PS/$HCO_3^-$ system, 0.1 μM BZF, 0.1 μM TMBA, and 0.2 μM NPX were added simultaneously as probe compounds for •OH, SO_4•$^-$, and CO_3•$^-$. In the UV/PS/NO_3^- system, 0.1 μM aniline (AN), sulfamethoxazole (SMX), and trimethoprim (TMP) were used as probes for •OH, SO_4•$^-$, and NO_2•. The concentration of primary and secondary radicals in the different systems was confirmed by monitoring the degradation rate constants of the probes in each system. Additionally, NEO degradation was examined in various actual waters: deionized water (DW, used as a control), river water (RW), and secondary sedimentation tank effluent from a sewage treatment plant (STPW).

To identify transformation products (TPs) of NEO, higher concentrations were used in the UV/PS system; specifically 50 μM NEO and 500 μM PS. Comparison of TPs under UV/PS, UV/H_2O_2/Cl^-, UV/H_2O_2/HCO_3^-, and UV/H_2O_2/NO_3^- with those under

194 the UV/H_2O_2 system was used to determine the proprietary TPs for SO_4•$^-$, Cl•, CO_3•$^-$,
195 and NO_2•. Acute and chronic toxicity of detected TPs to three ecologically significant
196 aquatic organisms (green algae, daphnia, and fish) was calculated using ECOSAR v2.2
197 software. In addition, *Vibrio fischeri* was used as a model microorganism and mixed
198 with reacted UV/PS solution (degradation of 5μM NEO by 50μM PS) to determine the
199 acute toxicity intensity of samples (see Text S2 for specific toxicity tests). All kinetic
200 experiments were repeated in triplicate.

201 *2.3 Analytical methods*

202 The concentrations of NEO and probe compounds were analyzed concurrently using
203 high-performance liquid chromatography coupled with tandem quadrupole mass
204 spectrometry (HPLC-tqMS, Agilent Technologies Co., USA). The analysis was
205 performed in either ESI negative or positive mode with a single injection volume of 10
206 μL. The instrument featured a C-18 column (2.1 × 100 mm, 1.8 μm, Agilent, ZORBAX
207 Eclipse Plus C18, USA). Chromatographic separation of the various substances was
208 achieved using gradient elution of methanol and 0.1% formic acid over 8 minutes at a
209 flow rate of 0.4 mL/min. Detailed information on the organic compound assays is
210 provided in Table S1.

211 TPs of NEO were analyzed using an UltiMate 3000 HPLC (Thermo Fisher, Waltham,
212 USA) coupled to tandem orbital ion trap high-resolution mass spectrometry (Orbitrap
213 HRMS, Thermo Fisher Scientific Co., USA) and an electrospray ion source (ESI). The
214 instrument used was equipped with the same C-18 column as the HPLC-tqMS, and
215 chromatographic separation was conducted at a flow rate of 0.4 mL/min with a gradient

elution time of 23 minutes. The single injection volume was 10 μL, and the instrument scanned in the range of 50−1000 m/z in ESI positive mode. Additional details of the various analytical instruments and their corresponding methods can be found in Text S3.

2.4 Kinetic model

According to the results of radical identification and the literatures, •OH and SO_4•$^-$ are the main radicals in UV/PS activated systems [46]. Based on the assumption of steady-state concentration, the simplified kinetic model for NEO degradation by UV/PS can therefore be expressed as follows:

$$k_{NEO} = k_{UV,\,NEO} + k_{\bullet OH,\,NEO}[\bullet OH]_{ss} + k_{SO_4\bullet^-,\,NEO}[SO_4\bullet^-]_{ss} \quad (1)$$

where k_{NEO} is the apparent pseudo-first-order rate constant (min^{-1}) for the degradation of NEO in UV/PS expressed using the Langmuir-Hinshelwood kinetic model (see Eq. (2) for the model); $k_{UV,\,NEO}$ is the apparent pseudo-first-order rate constant for the degradation of NEO under direct UV irradiation (min^{-1}), which is a low and negligible value; $k_{\bullet OH,\,NEO}$ and $k_{SO_4\bullet^-,\,NEO}$ are the second-order rate constants for NEO reaction with •OH and SO_4•$^-$ ($M^{-1}\ s^{-1}$); and $[\bullet OH]_{ss}$ and $[SO_4\bullet^-]_{ss}$ are the steady-state concentrations of •OH and SO_4•$^-$ (M).

$$k_{NEO} = k_{obs} = \frac{d\left[\ln C_0 / C_t\right]}{dt} \quad (2)$$

C_0 and C_t are the initial and remaining NEO concentrations. $R_{\bullet OH}$ and $R_{SO_4\bullet^-}$ represent the percentage contributions of •OH and SO_4•$^-$ (%), which are calculated using Eqs. (3)−(4).

$$R_{\bullet OH,\,NEO} = \frac{k_{\bullet OH,\,NEO}[\bullet OH]_{ss}}{k_{NEO}} \quad (3)$$

$$R_{SO_4^{\bullet-},\,NEO} = \frac{k_{SO_4^{\bullet-},\,NEO}[SO_4^{\bullet-}]_{ss}}{k_{NEO}} \quad (4)$$

In previous studies, the degradation kinetics were detected by liquid chromatography (LC) using two probes, usually nitrobenzene (NB) and p-chlorobenzoic acid (pCBA) to calculate $[\bullet OH]_{ss}$ and $[SO_4^{\bullet-}]_{ss}$, respectively [47]. However, the addition of higher concentration probes inevitably competes with target pollutants for free radicals, which reduces availability and thus affects overall results accuracy. On the other hand, the relatively low sensitivity and high detection limit of LC makes it impossible to reduce probe concentrations.

In all four systems of this study (UV/PS, UV/PS/Cl^-, UV/PS/HCO_3^-, and UV/PS/NO_3^-), low concentration probes were used and LC-tqMS with very low detection limits was utilised to detect probe concentrations and minimize competing effects on the system. These more stringent criteria for probe concentrations are favorable for improving the accuracy of the evaluation of radical concentrations and relative contributions.

In the UV/PS system, 0.1 μM of pCBA and BZF were used as probes. Probe selection conditions were: (1) the second-order rate constants of the probes and radicals were as similar as to those of NEO; (2) the probes were highly ionized in the mass spectra; and (3) the second-order rate constants were measured under stringent conditions. In addition, the correction for the second-order rate constant of the probe was performed using a competitive kinetics approach (see Text S4–S9 for details of the determination).

Subsequently, $[\bullet OH]_{ss}$ and $[SO_4\bullet^-]_{ss}$ were calculated by solving the probe kinetic model, Eqs. (5)−(6):

$$k_{pCBA} = k_{UV,\,pCBA} + k_{\bullet OH,\,pCBA}[\bullet OH]_{ss} + k_{SO_4\bullet^-,\,pCBA}[SO_4\bullet^-]_{ss} \quad (5)$$

$$k_{BZF} = k_{UV,\,BZF} + k_{\bullet OH,\,BZF}[\bullet OH]_{ss} + k_{SO_4\bullet^-,\,BZF}[SO_4\bullet^-]_{ss} \quad (6)$$

where k_{pCBA} and k_{BZF} are the k_{obs} for degradation of pCBA and BZF during UV/PS (min^{-1}); $k_{UV,\,pCBA}$ and $k_{UV,\,BZF}$ are the k_{obs} for the degradation of pCBA and BZF under direct UV irradiation (min^{-1}); $k_{\bullet OH,\,pCBA}$ and $k_{\bullet OH,\,BZF}$ are the second-order rate constants for the reaction of pCBA and BZF with •OH ($M^{-1}\ s^{-1}$); and $k_{SO_4\bullet^-,\,pCBA}$ and $k_{SO_4\bullet^-,\,BZF}$ are the second-order rate constants for the reactions of pCBA and BZF with $SO_4\bullet^-$ ($M^{-1}\ s^{-1}$).

In the UV/PS/Cl^- system, radicals that mainly play a role in degrading pollutants include •OH, $SO_4\bullet^-$, Cl•, and $Cl_2^-\bullet$ [48]. Based on our previous study [49] and recent advances in probe-based methods [48], we selected 0.1 μM pCBA, BZF, TMBA, and 0.2 μM NPX as probes and constructed kinetic models to calculate the concentration of radicals in the system (see Text S10 for specific models and calculation details). Similarly, the concentrations of primary and secondary radicals in the UV/PS/HCO_3^- and the UV/PS/NO_3^- systems were modeled by similar probe-based kinetic models, and the computational details are shown in Text S11 and S12, respectively. The second-order rate constants of all probes and NEO with radicals are summarized in Table S2.

It should be noted that the concentration of probe NPX (0.2 μM) was higher than the other probes (0.1 μM) due to the fact that both primary and secondary radicals have higher second-order rate constants with NPX, making it difficult to capture accurate

kinetic profiles at lower concentrations.

2.5 Theoretical calculation methods

Quantum chemical calculations were performed in the same way as in our previous study [49], using Gaussian 16 A.03 and Multiwfn 3.8 [50]. The condensed Fukui function (CFF), the highest occupied molecular orbital (HOMO), and the lowest unoccupied molecular orbital (LUMO) were analyzed using density flooding theory (DFT). Detailed information on the calculations is given in Text S13.

2.6 Statistical analysis

Spearman's correlation analysis and one-way analysis of variance (ANOVA) were conducted using IBM SPSS version 19.0. All plots were generated using Origin 2022 software.

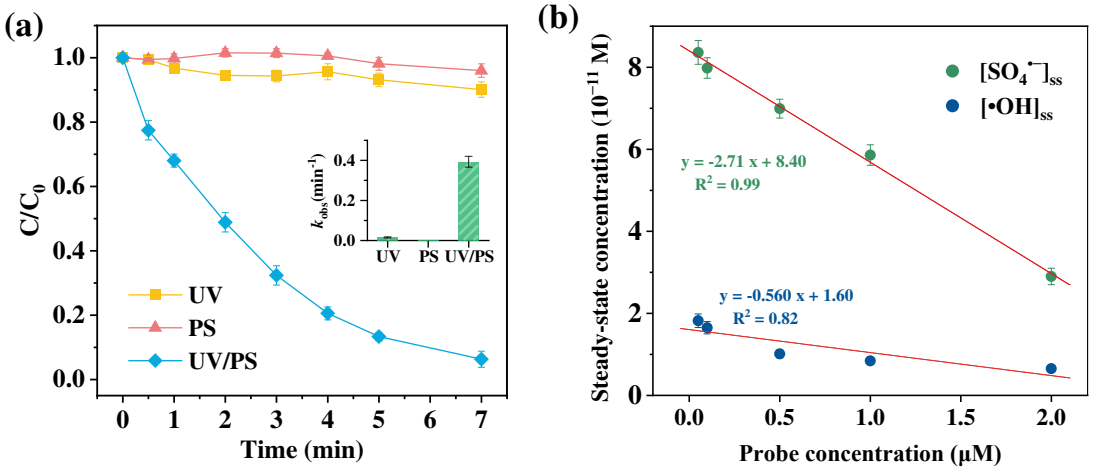

Fig. 1. (a) Degradation of NEO with sole PS in dark conditions, UV irradiation and UV/PS (Inset: the value of k_{obs} under different conditions); (b) linear relationships between the probe (pCBA and BZF) concentrations and determined steady-state

concentrations of •OH and SO_4•$^-$ in the UV/PS system. Conditions: [PS]= 50 μM, [NEO]= 5 μM, pH=7.

3. Results and discussion

3.1. Degradation kinetics of NEO in pure water

The degradation of NEO was assessed using PS, direct UV, and the UV/PS system. As depicted in Fig. 1, the removal of NEO with PS or UV alone was negligible over 7 min. However, the UV/PS system exhibited rapid degradation of NEO, with nearly 93.7% of NEO decomposed within 7 min. The degradation process in the UV/PS system followed pseudo-first-order kinetics, with k_{obs} of 0.393 min^{-1} and R^2 value of 0.998. In addition, in order to assess the mineralization of the UV/PS system for the pollutants, the removal of TOC during degradation was tested. The results showed that the removal efficiency of TOC was lower than the degradation of NEO, but was able to remove 53.9% of TOC in 30 min (Fig. S3). Although complete mineralization of contaminants is very difficult, the UV/PS system achieved an acceptable level of mineralization capacity for NEO. The UV/PS system achieved a relatively high level of mineralization compared to other UV-AOPs [51,52].

The rapid degradation of NEO by UV/PS has been attributed to the involvement of highly reactive oxidizing radicals in this process. After quenching experiments (including tert-butanol and methanol) and EPR analysis, radicals in UV/PS contained •OH and SO_4•$^-$ (see Text S14 and Fig. S4 for related identification analysis). In order to investigate $[•OH]_{ss}$ and $[SO_4•^-]_{ss}$ in the system, probe compounds were added to

318 construct kinetic models. Probe addition usually affects the free radical concentration
319 by changing the free radical chemistry in the system. We investigated the free radical
320 concentration of the system at probe additions of 0.05−2.0 μM (Fig. 1b). It was found
321 that $[\bullet OH]_{ss}$ and $[SO_4\bullet^-]_{ss}$ depend on the concentration of the probe used. With an
322 increase in probe concentration from 0.05 to 2.0 μM, $[\bullet OH]_{ss}$ and $[SO_4\bullet^-]_{ss}$ decreased
323 linearly from 1.82×10^{-11} and 8.36×10^{-11} M to 0.65×10^{-11} and 2.90×10^{-11} M,
324 respectively. However, the precision of probe degradation curve determination
325 decreased when the probe concentration was lower. To address these issues, we used a
326 mass spectrometry technique with lower detection lines, which were reduced to 32 and
327 11 ng/L for probes pCBA and BZF. Therefore, after balancing the effect of the probes
328 on the radicals and the instrumental detection accuracy required for the concentration
329 determination, we used 0.1 μM as the standard concentration of probes in the study.
330 After calculation, $[\bullet OH]_{ss}$ and $[SO_4\bullet^-]_{ss}$ in UV/PS was 1.65×10^{-11} M and 7.98×10^{-11}
331 M, and their percentage contribution to NEO degradation was 37.6% and 62.4%,
332 respectively.

333 Under similar UV conditions, the low concentration probe method applied in this
334 study (probe concentration of 0.1 μM) detected 1.9−51.4 times higher concentrations
335 of radicals in the UV/PS system compared to the literature (probe concentration of
336 1.0−10.0 μM) [46,53,54]. Similarly, a similar phenomenon was found in the UV/H_2O_2
337 system, where $[\bullet OH]_{ss}$ determined using a 0.1 μM probe was more than twice as high
338 as that determined using a 1.0 μM probe [38]. In summary, excessive probe
339 concentration can seriously introduce errors in the determination of radical

concentration by exacerbating the competitive depletion of radicals [38]. To ensure the accuracy of radical concentration identification, the probe concentration should be selected in favor of the lower concentration as much as possible.

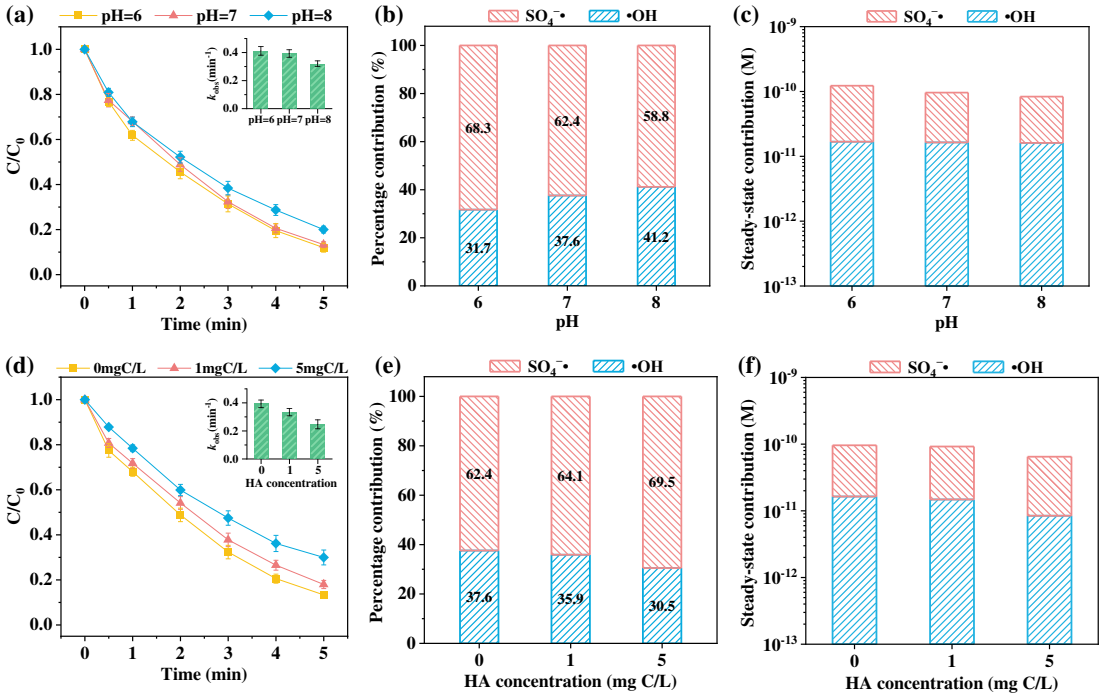

Fig. 2. Effects of pH (a) and humic acid (HA, d) (Inset: the relationship between pH, HA and the value of k_{obs}) in the degradation of NEO in the UV/PS system; trends in percentage contributions of radicals to NEO degradation during UV/PS at different pH (b) and HA (e); trends in steady-state concentration of radicals to NEO degradation during the UV/PS system at different pH (c) and HA (f). Conditions: [PS] = 50 μM, [NEO] = 5 μM.

3.2. Effect of pH and NOM on NEO degradation

3.2.1 pH

NEO degradation during UV/PS experiments showed a notable dependence on pH

355 over the range of 6 to 8 (Fig. 2a). The k_{obs} for NEO decreased from 0.412 to 0.321 min^{-1}
356 as pH increased over this range. This suggests UV/PS degradation of NEO is more
357 favorable at lower pH.

358 The impact of pH on NEO degradation during UV/PS experiments is multifaceted.
359 First, dissociation of PS in aqueous solution is enhanced only under strongly acidic
360 conditions, and its quantum efficiency of photo-dissociation remains stable at different
361 pH [55]. Therefore, the effect of dissociation of PS at different pH on the system may
362 be excluded. In addition, pH influences the dissociation of NEO. The dissociation
363 constants (pK_a) of NEO were determined as 3.01 and 8.02. At pH 6 and 7, NEO exists
364 as a neutral molecule, while at pH 8, 50% of NEO molecules are in an anionic form
365 (Fig. S5). It has been reported that organic compounds (e.g., edaravone) in the anionic
366 form may be more reactive with radicals [56]. However, the uniform decrease in k_{obs}
367 with increasing pH demonstrates this fraction of NEO anions has less promotional
368 effect on degradation. Furthermore, pH impacted on radicals and their transformations.
369 As pH increased from 6 to 8, $[\bullet OH]_{ss}$ remained relatively stable, decreasing only from
370 1.68×10^{-11} to 1.61×10^{-11} M, while $[SO_4\bullet^-]_{ss}$ decreased from 1.06×10^{-10} to $6.72 \times$
371 10^{-11} M (Fig. 2c). Meanwhile, the proportion of $SO_4\bullet^-$ decreased from 68.3% to 58.8%
372 and that of •OH increased from 31.7% to 41.2% (Fig. 2b). In alkaline environments,
373 radicals may be captured by OH^-, resulting in a decrease in overall radical concentration
374 (Eqs. (7) and (8)). Meanwhile, $SO_4\bullet^-$ is partially transformed as •OH after being
375 captured by OH^-, which compensates for the partial quenching effect originally
376 suffered by •OH, and thus $[\bullet OH]_{ss}$ is relatively stable. pH also affects the redox potential

of radicals. Based on the Nernst equation the redox potential of •OH decreases with increasing pH, which leads to a higher oxidizing capacity of •OH under acidic conditions thus promoting NEO degradation.

$$SO_4^{\bullet-} + OH^- \rightarrow SO_4^{2-} + \bullet OH \quad (7)$$

$$\bullet OH + OH^- \rightarrow O^{-}\bullet + H_2O \quad (8)$$

3.2.2 NOM

As shown in Fig. 2d, the presence of HA inhibited NEO degradation. As HA concentration increased (0 to 5 mg C/L), k_{obs} for NEO decreased from 0.393 to 0.247 min^{-1}. The inhibitory role of HA can be assigned to two main factors: (1) Inner Filtering Effects during which HA's chromophores reduce the photon dose absorbed by PS due to competitive absorption, leading to decreased formation of •OH and $SO_4^{\bullet-}$; and (2) Radical Scavenging in which HA scavenges various radicals in the system. As HA concentration increased from 0 to 5 mg C/L, $[\bullet OH]_{ss}$ and $[SO_4^{\bullet-}]_{ss}$ decreased from 1.65 × 10^{-11} to 8.43 × 10^{-12} M and from 7.98 × 10^{-11} to 5.63 × 10^{-11} M, respectively (Fig. 2f). Notably, $SO_4^{\bullet-}$ plays a more significant role in NEO degradation in the presence of HA. As HA concentration increased, the contribution of $SO_4^{\bullet-}$ to the degradation process increased from 62.4% to 69.5%, while the contribution of •OH decreased from 37.6% to 30.5% (Fig. 2e). Compared to $[SO_4^{\bullet-}]_{ss}$ (29.4%), $SO_4^{\bullet-}$ suffered a greater inhibitory effect (48.9%). These results are attributed to the fact that the second-order rate constants for the reaction of •OH with HA (1.21−6.50 × 10^8 M^{-1} s^{-1}) are much higher than those of $SO_4^{\bullet-}$ (0.64−3.68 × 10^7 M^{-1} s^{-1}), thus producing a more pronounced quenching effect on •OH. In addition, recent studies have shown that HA may convert

organic radicals after hydrogen atom abstraction of pollutants, and cationic radicals after deprotonation of neutral radicals to the pollutant proper, Eq. (9). Since its reaction rate constant is 6.50×10^8 M^{-1} s^{-1}, this may also be one of the key factors in the inhibition of NEO degradation by HA.

$$NEO(-H)\bullet + HA + H_2O \rightarrow NEO + HA_{\text{oxidation state}} + OH^- \quad (9)$$

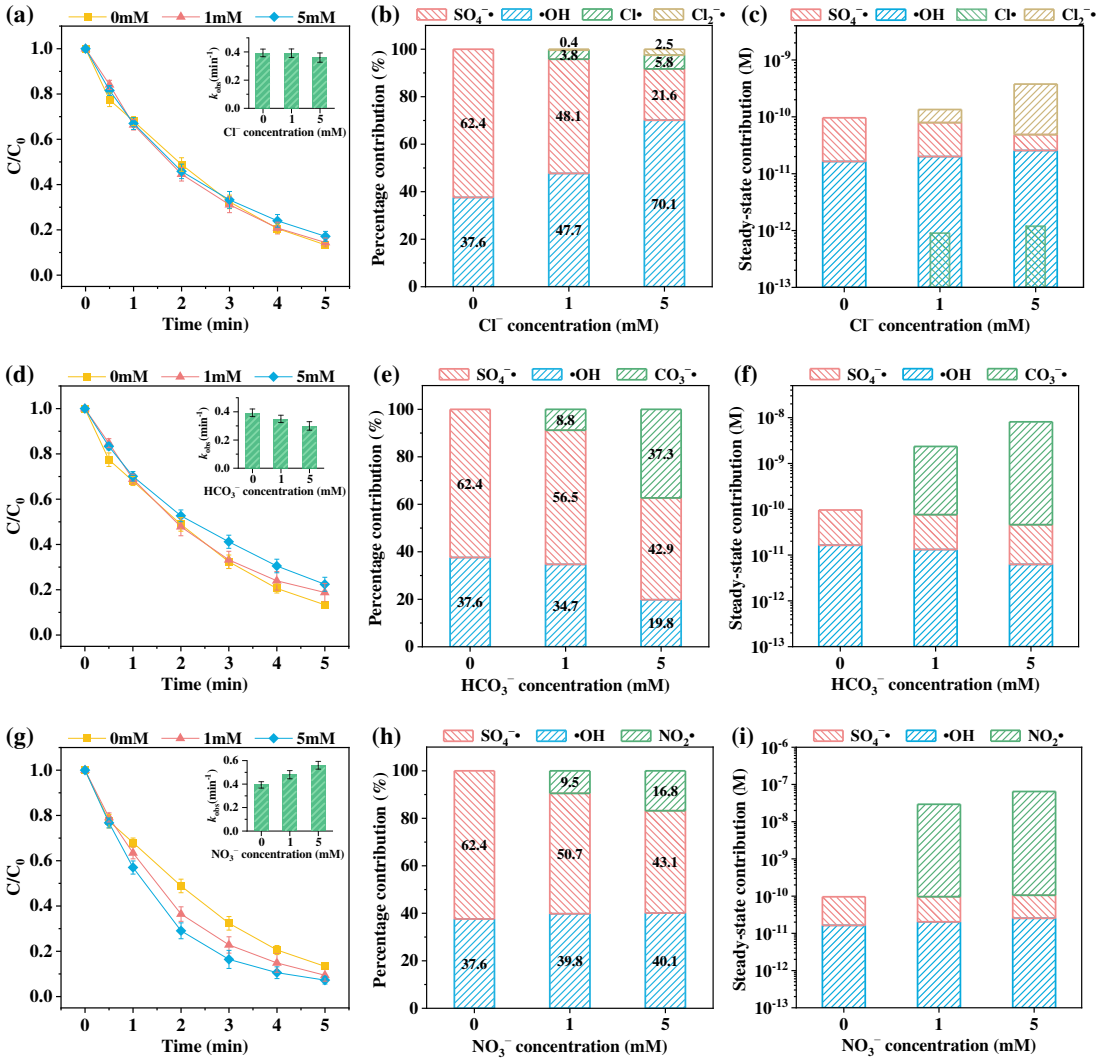

Fig. 3. Effects of (a) Cl^-, (d) HCO_3^-, and (g) NO_3^- (Inset: the relationship with Cl^-, HCO_3^-, and NO_3^- and the value of k_{obs}) in the degradation of NEO during UV/PS; trends in percentage contributions of radicals to NEO degradation during UV/PS at

409 different (b) Cl^-, (e) HCO_3^-, and (h) NO_3^- concentrations; trends in steady-state
410 concentration of radicals to NEO degradation during UV/PS at different (c) Cl^-, (f)
411 HCO_3^-, and (i) NO_3^- concentrations. Conditions: [PS] = 50 μM, [NEO] = 5 μM, pH =
412 7.
413
414 *3.3. Effect of inorganic anions on NEO degradation and radical contribution*
415 Inorganic anions are common background substances in a variety of natural waters
416 including river water, tap water and groundwater. Their widespread presence may alter
417 the types and radical concentrations during UV/PS, and directly impact the removal of
418 pollutants. Therefore, the effects of inorganic anions on NEO degradation in UV/PS
419 systems were investigated, and the types and concentrations of secondary radicals
420 (including Cl•, Cl_2^-•, CO_3•$^-$, and NO_2•) produced in the system were analyzed by probe-
421 based kinetic models.
422 *3.3.1 Cl^-*
423 As illustrated in Fig. 3a, the presence of 1 mM Cl^- had minimal impact on NEO
424 degradation. However, as Cl^- concentration increased from 1 to 5 mM, NEO
425 degradation became inhibited. As Cl^- concentration increased from 0 to 1 mM, k_{obs}
426 decreased slightly from 0.393 to 0.391 min^{-1}, and as Cl^- concentration was further
427 increased to 5 mM the k_{obs} value decreased to 0.360 min^{-1}. Cl^- in the environment
428 converts radicals (•OH and SO_4•$^-$) to a variety of reactive chlorine species including
429 Cl•, Cl_2^-•, and $ClOH^-$•, as shown in Eqs (10)−(13). The rapid decomposition of $ClOH^-$•
430 (Eqs. (14) and (15)) leads to steady-state concentration usually below 10^{-16} M, and the

system reactive chlorine species (RCS) are dominated by Cl• and Cl_2^{-}• [34]. For obtaining specific information about free radical transformation, kinetic models were constructed using NPX, pCBA, BZF, and TMBA as probes to calculate $[•OH]_{ss}$, $[SO_4•^-]_{ss}$, $[Cl•]_{ss}$, and $[Cl_2^-•]_{ss}$ during UV/PS/Cl^- system. The results illustrated that $[SO_4•^-]_{ss}$ decreased from 7.98×10^{-11} M to 5.91×10^{-11} M, but $[•OH]_{ss}$ increased from 1.65×10^{-11} M to 2.00×10^{-11} M in the system when Cl^- concentration was 1mM (Fig. 3c). Meanwhile, $[Cl•]_{ss}$ and $[Cl_2^-•]_{ss}$ were produced in the system with concentrations of 8.98×10^{-13} M and 5.53×10^{-11} M. At this point, Cl^- in the system scavenges $SO_4•^-$ to form Cl•, Cl_2^-•, and $ClOH^-$• which subsequently decomposes to •OH. The generation of •OH (7.71×10^9 M^{-1} s^{-1}) and highly reactive Cl• (1.38×10^{10} M^{-1} s^{-1}) compensated for the reduction of $[SO_4•^-]_{ss}$, resulting in a reduced effect of low concentrations of Cl^- on NEO degradation. At 1 mM Cl^- concentration, the $SO_4•^-$ contribution to NEO degradation was reduced from 62.4% to 48.1%, while the •OH contribution increased from 37.6% to 47.7% (Fig. 3b). The newly generated Cl• and Cl_2^-• radicals contributed 3.8% and 0.4% to NEO degradation, respectively. When the Cl^- concentration was increased to 5 mM it promoted further conversion of $SO_4•^-$ to Cl• and Cl_2^-•. The concentrations of $[Cl_2^-•]_{ss}$ and $[Cl•]_{ss}$ increased to 3.28×10^{-10} M and 1.19×10^{-12} M, which were 1.33- and 5.93-fold increases compared to that at 1mM Cl^- concentration, respectively. NEO degradation at this point was reduced due to the large decrease in $[SO_4•^-]_{ss}$ and the relatively low reactivity of the newly generated Cl_2^-• with NEO (2.14×10^7 M^{-1} s^{-1}). The $SO_4•^-$ contribution to NEO degradation decreased to 21.6%, and the contribution of generated Cl_2^-• was only 2.5%.

$$SO_4^{\bullet -} + Cl^- \rightarrow SO_4^{2-} + Cl\bullet \quad (10)$$

$$Cl\bullet + Cl^- \rightarrow Cl_2^-\bullet \quad (11)$$

$$\bullet OH + Cl^- \rightarrow ClOH^-\bullet \quad (12)$$

$$ClOH^-\bullet + Cl^- \rightarrow Cl_2^-\bullet + OH^- \quad (13)$$

$$ClOH^-\bullet \rightarrow Cl^- + \bullet OH \quad (14)$$

$$ClOH^-\bullet + H^+ \rightarrow Cl\bullet + H_2O \quad (15)$$

3.3.2 HCO_3^-

HCO_3^- inhibited NEO degradation during UV/PS system, and the inhibitory effect was enhanced with increasing HCO_3^- concentration (Fig. 3d). As HCO_3^- concentration was increased from 0 to 1 mM, k_{obs} decreased from 0.393 min^{-1} to 0.350 min^{-1}. When the concentration of HCO_3^- was further increased to 5 mM, the k_{obs} decreased to 0.301 min^{-1}. As shown in Eqs. (16)–(17), HCO_3^- will produce $CO_3\bullet^-$ radicals by competing for •OH and $SO_4\bullet^-$ [36,57]. Thus, radicals in UV/PS systems were altered in two ways: First, quenching of the original radicals. As HCO_3^- concentration increased from 0 to 5 mM, $[\bullet OH]_{ss}$ and $[SO_4\bullet^-]_{ss}$ decreased from 1.65×10^{-11} to 6.27×10^{-12} M and from 7.98×10^{-11} to 3.97×10^{-11} M i.e., by 61.8% and 50.3%, respectively (Fig. 3f). Second, conversion of radicals. In order to obtain specific information on transformation between radicals, kinetic models were constructed using NPX, BZF and TMBA as probes to collectively calculate $[\bullet OH]_{ss}$ and $[SO_4\bullet^-]_{ss}$, and $[CO_3\bullet^-]_{ss}$ in UV/PS/HCO_3^-. The results showed that $[CO_3\bullet^-]_{ss}$ in the system was 2.28×10^{-9} M and 8.07×10^{-9} M when HCO_3^- concentration was 1 mM and 5 mM, respectively. Meanwhile, $CO_3\bullet^-$ also played a partial contribution in degradation of NEO, and the percentage contribution of

$CO_3^{\bullet-}$ to NEO degradation was 8.8% and 37.3% when the HCO_3^- concentration was 1 and 5 mM, respectively (Fig. 3e). However, $CO_3^{\bullet-}$ has significant selectivity for organic compounds. Although $CO_3^{\bullet-}$ has relatively higher reactivity (10^6–10^7 M^{-1} s^{-1}) with electron-rich micropollutants such as nitrogen-containing and aromatic compounds, it is still about two orders of magnitude lower than that of •OH and $SO_4^{\bullet-}$ [58,59]. Therefore, the generation of $CO_3^{\bullet-}$ prolongs the chain reaction of radicals and reduces the overall oxidizing capacity of the system.

$$HCO_3^- + SO_4^{\bullet-} \rightarrow HCO_3^{\bullet} + SO_4^{2-} \quad (16)$$

$$HCO_3^- + {\bullet}OH \rightarrow CO_3^{\bullet-} + H_2O \quad (17)$$

3.3.3 NO_3^-

The effect of NO_3^- concentration (0−5 mM range) on NEO degradation is shown in Fig. 3g. All concentrations of NO_3^- enhanced NEO degradation, with k_{obs} increasing from 0.393 to 0.560 min^{-1} as NO_3^- concentration increased from 0 to 5 mM. The enhanced removal of NEO was mainly due to the following reasons: First, photoexcitation generates new radicals. NO_3^- absorbs UV irradiation and generates NO_2• and O^{-}•, Eqs. (18)–(20) [60]. Subsequently, O^{-}• reacts with water to form •OH which enhances NEO oxidation. In contrast to other highly unstable reactive nitrogen species (RNS, e.g., ONOOH and NO•), NO_2• is considered the only stable RNS in the presence of NO_3^-. Therefore, SMX, AN, and TMP were used as probes to construct kinetic models to study the species, transformations, and concentrations of radicals in the UV/PS/NO_3^- system. The results showed that $[NO_2{\bullet}]_{ss}$ was 2.93×10^{-8} M and 6.45×10^{-8} M when NO_3^- concentration in the system was 1 and 5 mM, respectively (Fig.

3i). Although the $k_{NO_2\bullet\ NEO}$ was relatively limited (1.28×10^6 M^{-1} s^{-1}), the higher $[NO_2\bullet]_{ss}$ still promoted degradation of NEO with $NO_2\bullet$ contributing 9.5% (1 mM NO_3^-) and 16.9% (5 mM NO_3^-) (Fig. 3h). Meanwhile, $[\bullet OH]_{ss}$ in the system increased to 2.04×10^{-11} M and 2.55×10^{-11} M in the presence of 1 and 5 mM NO_3^-, respectively. Second, NO_3^- also absorbs UV to generate O_2 and NO_2^- [49]. O_2 in UV/PS can be involved in the production of radicals through several pathways [61]. Third, limited quenching effect. Among other inorganic anions such as Cl^- and HCO_3^-, NO_3^- reacts with •OH ($k_{\bullet OH,\ NO_3^-} < 1 \times 10^5$ M^{-1} s^{-1}) and $SO_4\bullet^-$ ($k_{SO_4\bullet^-,\ NO_3^-} = 2.1 \times 10^0$ M^{-1} s^{-1}) with the smallest reaction rate, and the quenching effect on radicals was accordingly weak [62]. Fourth, minimal effects of UV luminous flux. Unlike far-UVC, there is little overlap between 254 nm UV and the NO_3^- absorption band, so the level of UV absorption shielding caused by NO_3^- is low [62].

$$NO_3^- + h\nu \rightarrow NO_2\bullet + O^-\bullet \quad (18)$$

$$O^-\bullet + H_2O \rightarrow \bullet OH + OH^- \quad (19)$$

$$NO_3^- + h\nu \rightarrow NO_2^- + 0.5\ O_2 \quad (20)$$

3.4. NEO degradation in actual waters

The degradation of NEO by UV/PS in different actual waters (including DW, RW and STPW) is shown in Fig. 4a (see Table S3 for details of water quality). The k_{obs} of NEO degradation during UV/PS were in the order of DW (0.393 min^{-1}) > RW (0.098 min^{-1}) > STPW (0.071 min^{-1}). The main reasons include: (1) the chromaticity of actual waters may affect UV flux, which in turn reduces the generation of radicals; and (2) the presence of NOM and inorganic anions quenches radical availability. As mentioned

earlier, background ions in actual waters may significantly inhibit NEO degradation by scavenging radicals.

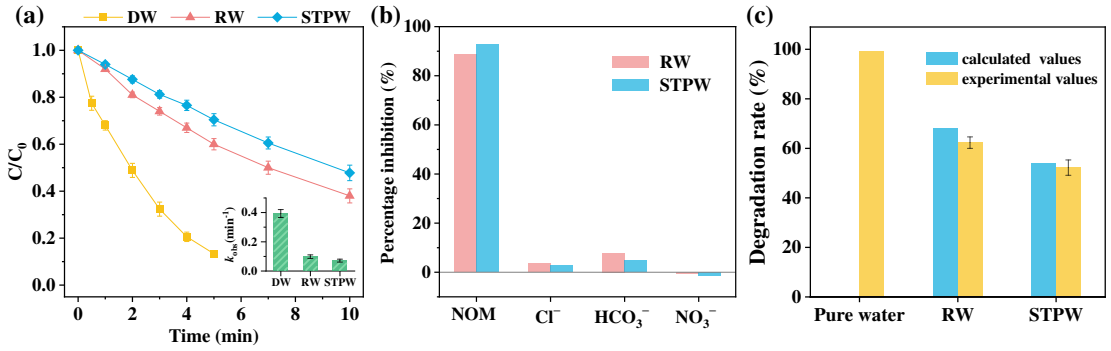

Fig. 4. (a) Degradation of NEO during UV/PS in actual waters (inset: the relationship with actual waters and the value of k_{obs}); (b) percentage contribution of NOM and inorganic anions to NEO inhibition in actual waters; (c) degradation rate after 10 min of degradation in the UV/PS process and predicted values of NEO degradation in actual waters. Conditions: [PS] = 50 μM, [NEO] = 5 μM, pH = 7; DW = deionized water, RW = river water and STPW = sewage treatment plant water.

In order to specifically analyze the main inducing factors for the attenuation of the degradation effect we correlated the k_{obs} with organic matter (COD and TOC), pH, inorganic anions (Cl^-, HCO_3^-, NO_3^-, and SO_4^-), and typical cations (Ca^{2+}, Mg^{2+}, Na^+, K^+, NH_4^+) in the actual waters. Spearman's correlation analysis was used to determine the relevant information since the parameters of the actual waters and k_{obs} do not obey a normal distribution. The results were shown in Fig. S6, where organic matter (i.e., NOM as described previously) in water was the main factor inhibiting NEO degradation. In addition, the specific roles of different water matrix components in the UV/PS

system in real waters were traced by simulating the theoretical inhibitory (promotion) effects produced by the water matrix components, and determining their contribution in the total inhibition rate (the sum of inhibition rates of all water matrix components). Among them, impact of water matrix (NOM and inorganic anions) was predicted by interpolating their concentrations in the matrix effect fitting curves (determined by sections 3.2 and 3.3; these results are illustrated in Fig. S7). The results show that although NO_3^- promotes the degradation of NEO, the promotion effect is limited (only 0.6−1.3%). The inhibitory effects of NOM accounted for nearly 90% of the total effect, which was 11.4−34.7 times more than the effects of Cl^- and HCO_3^- (Fig. 4b). The above phenomenon was attributed to the fact that the sampling site was a major residential area in Beijing, where anthropogenic activities resulted in relatively high concentrations of NOM in actual waters. However, within 10 min, NEO in RW and STPW could still be degraded by 62.3% and 53.3% in the UV/PS system, respectively. Although NEO degradation in actual waters is not as effective as in DW, more than 53% NEO reduction can still be achieved within 10 min.

In addition, a prediction model for degradation rate of NEO in actual waters was constructed based on four major water quality factors, including NOM (x_1), Cl^- (x_2), HCO_3^- (x_3), and NO_3^- (x_4) (see Text S15 and Table S4 for specific model construction details) [63]. The output kinetic model is shown in Eq. (21), where the coefficients of the primary terms can be considered as the weights of the influence of water quality factors. The results again demonstrate that NOM is the main factor influencing the degradation of NEO, followed by HCO_3^-. The model can also predict well the

degradation of NEO in actual waters. As shown in Fig. 4c, the calculated values are lower than the experimental values, which is probably due to the complex composition of NOM and the different reactivity of different substances with radicals. In addition, other inorganic ions (e.g., NO_2^-, Br^-, etc.) and other reducing substances in actual waters can also cause partial depletion of radicals.

$$Y = 98.9 - 2.071\,x_1 - 0.656\,x_2 - 1.099\,x_3 + 0.489\,x_4 - 0.382\,x_1x_2 - 0.192\,x_1x_3 + 0.176\,x_1x_4 + 0.369\,x_2x_3 + 0.312\,x_2x_4 + 0.187\,x_3x_4 \quad (21)$$

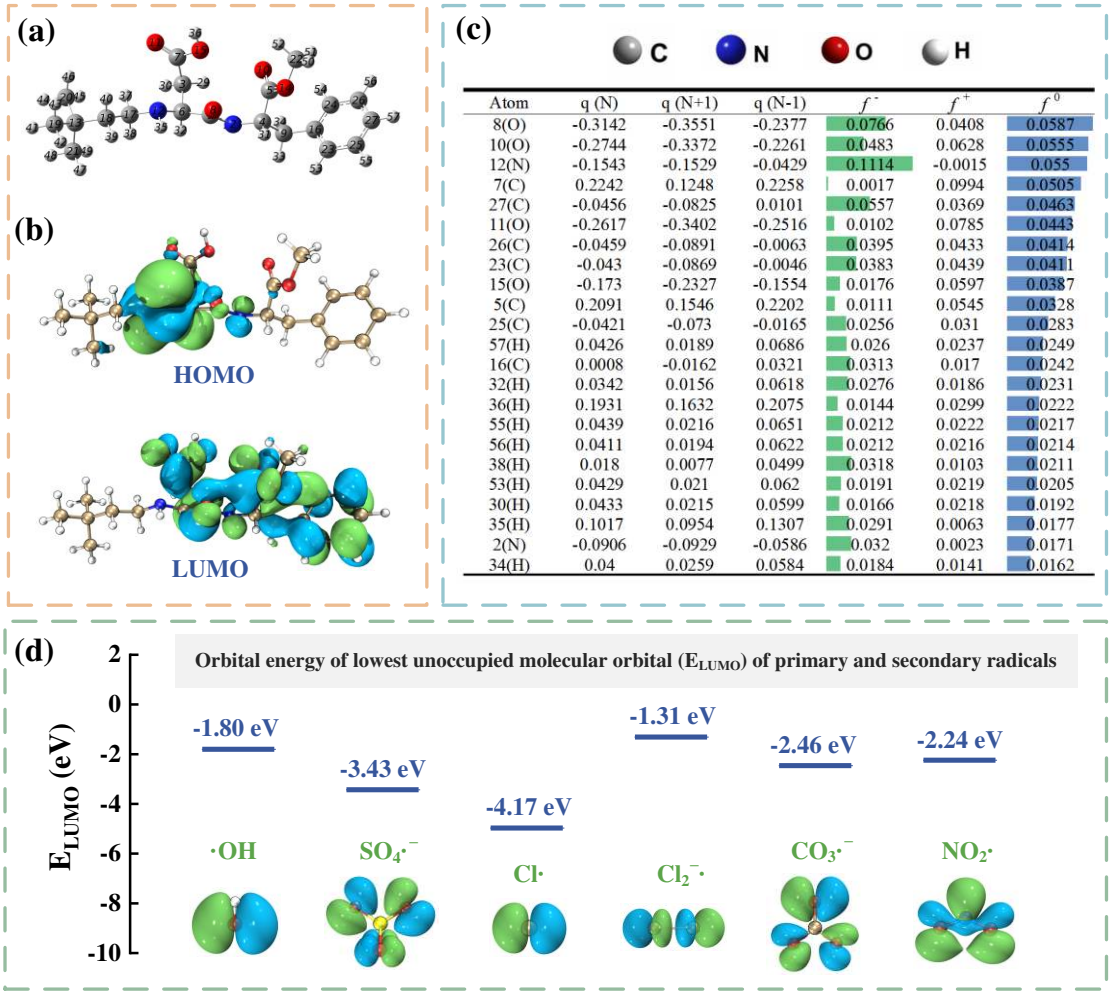

Atom	q (N)	q (N+1)	q (N-1)	f^-	f^+	f^0
8(O)	-0.3142	-0.3551	-0.2377	0.0766	0.0408	0.0587
10(O)	-0.2744	-0.3372	-0.2261	0.0483	0.0628	0.0555
12(N)	-0.1543	-0.1529	-0.0429	0.1114	-0.0015	0.055
7(C)	0.2242	0.1248	0.2258	0.0017	0.0994	0.0505
27(C)	-0.0456	-0.0825	0.0101	0.0557	0.0369	0.0463
11(O)	-0.2617	-0.3402	-0.2516	0.0102	0.0785	0.0443
26(C)	-0.0459	-0.0891	-0.0063	0.0395	0.0433	0.0414
23(C)	-0.043	-0.0869	-0.0046	0.0383	0.0439	0.0411
15(O)	-0.173	-0.2327	-0.1554	0.0176	0.0597	0.0387
5(C)	0.2091	0.1546	0.2202	0.0111	0.0545	0.0328
25(C)	-0.0421	-0.073	-0.0165	0.0256	0.031	0.0283
57(H)	0.0426	0.0189	0.0686	0.026	0.0237	0.0249
16(C)	0.0008	-0.0162	0.0321	0.0313	0.017	0.0242
32(H)	0.0342	0.0156	0.0618	0.0276	0.0186	0.0231
36(H)	0.1931	0.1632	0.2075	0.0144	0.0299	0.0222
55(H)	0.0439	0.0216	0.0651	0.0212	0.0222	0.0217
56(H)	0.0411	0.0194	0.0622	0.0212	0.0216	0.0214
38(H)	0.018	0.0077	0.0499	0.0318	0.0103	0.0211
53(H)	0.0429	0.021	0.062	0.0191	0.0219	0.0205
30(H)	0.0433	0.0215	0.0599	0.0166	0.0218	0.0192
35(H)	0.1017	0.0954	0.1307	0.0291	0.0063	0.0177
2(N)	-0.0906	-0.0929	-0.0586	0.032	0.0023	0.0171
34(H)	0.04	0.0259	0.0584	0.0184	0.0141	0.0162

Fig. 5. (a) Molecular construction of NEO after optimization; (b) HOMO and LUMO distribution of NEO; (c) partial Hirshfeld charge distribution and CFF index; and (d) Orbital energy of LUMO (E_{LUMO}) of primary and secondary radicals.

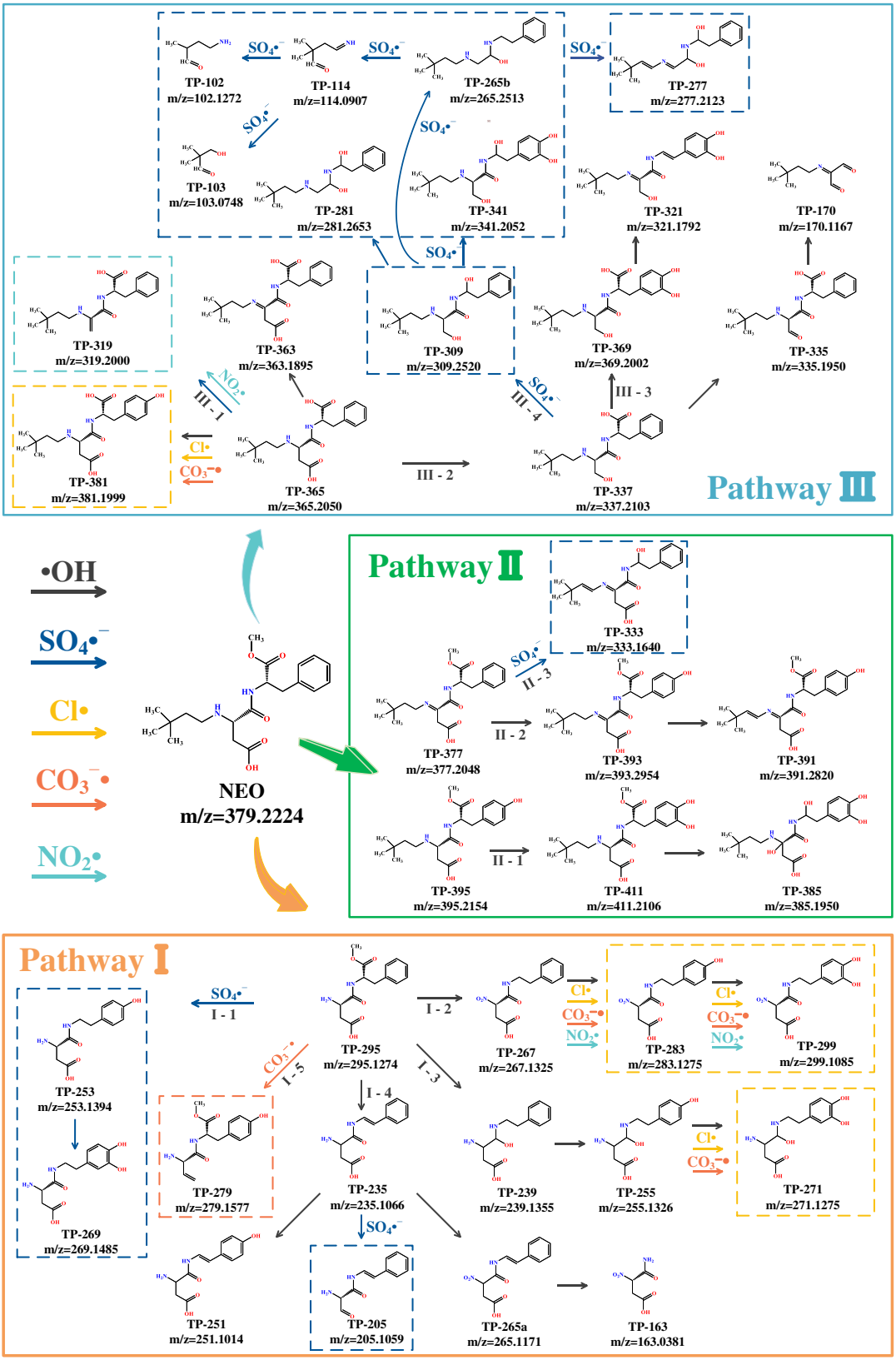

Fig. 6. Potential transformation products (TPs) and degradation pathways of NEO during UV/PS.

574 *3.5. Potential transformation products and degradation pathways of NEO*

575 In order to elucidate the potential degradation pathways of NEO, 39 TPs generated
576 during UV/PS experiments were identified using HPLC/Orbitrap HRMS, of which 33
577 TPs were found for the first time and are reported in this paper. Table S5 summarizes
578 TP various parameters such as detected molecular mass, molecular formula, magnitude
579 of error, number of peaks, and retention time for all potential degradation products. The
580 mass spectra and extracted ion chromatograms (EIC) of NEO and its TPs are illustrated
581 in Figs. S8−S46. To further identify the degradation sites of NEO, HOMO, LUMO,
582 Fukui function (f^0) and pairwise descriptors (Δf) were calculated using DFT and
583 Multiwfn software, and the results are illustrated in Fig. 5 (Text S16) [50,64]. The
584 HOMO orbitals were significantly concentrated near 12N and amide bonds (Fig. 5b).
585 It is hypothesized that the two C-N bonds and amide bond sites of 12N were the main
586 reaction sites of NEO during UV/PS degradation processes. The values of f^-, f^+, and f
587 ^{0} reflect the propensity of micropollutant molecules to be targeted by electrophiles,
588 nucleophiles and radicals, respectively (Fig. 5c) [27]. The magnitude of these values
589 represent the likelihood of the site being attacked [65]. •OH and SO_4•$^-$ are strong
590 electrophilic radicals, and mainly attack NEO electrophilically and through radical
591 attack [31]. Thus, the 12N and O atoms close to the amide bonds have the highest f^-
592 and f^0; this is the site most susceptible to electron loss and free radical attack, and is
593 consistent with the electron-loss positions described by HOMO.

594 Degradation pathways of NEO during UV/PS experiments were proposed based on
595 the measured TPs and DFT calculations. As shown in Fig. 6, three degradation

pathways were classified according to the initiating occurring functional groups of the degradation reaction, namely 5C-12N bond breaking (pathway I), hydrogen atom abstraction/hydroxylation (pathway II), and ester hydrolysis (pathway III). In addition, the UV/H_2O_2 system was used as a generator of •OH. UV/H_2O_2/Cl^-, UV/H_2O_2/HCO_3^-, and UV/H_2O_2/NO_3^- systems were used as generators of •OH and anionic radicals (Cl•, Cl_2^-•, CO_3•$^-$, and NO_2•, respectively). The attack tendencies of primary and secondary radicals in degrading NEO were distinguished by comparing the generation of TPs in different systems. The results illustrated that there were differences in the propensity of different species of radicals to attack NEO [45]: •OH was mainly involved in NEO degradation through hydroxylation, hydrogen atom abstraction (HAA), amine oxidation, ester hydrolysis, amide hydrolysis, and direct oxidation reactions, whereas SO_4•$^-$ was mainly involved in hydroxylation, HAA, decarboxylation, dehydration reactions, and demethylation to attack NEO. Cl•, CO_3•$^-$, and NO_2• are involved in the degradation of NEO through single electron transfer-mediated HAA, decarboxylation, and dehydration reactions.

Pathway I. Due to the highest f^- (0.1114) with 12N of the alkyl side chain, it is suggested that this is the most susceptible oxidation site for electrophilic attack. Pathway I therefore begins with the conversion of NEO to TP-295 by C-N bond breakage at 12N. In the subsequent oxidation processes there are five secondary degradation pathways, which are named as pathways I-1 to I-5, respectively. First, when the ester group attached to 5C of TP-295 is converted to a carboxyl group *via* a hydrolysis reaction, it may be further converted to the precursor substance TP-253 by

618 a SO_4•$^-$ driven decarboxylation reaction. Subsequently, 57H on the benzene ring is the
619 most likely to be converted to TP-253 by hydroxylation, due to the highest f^- and f^0.
620 However, TP-253 was not detected during UV/H_2O_2 experiments. In other words, the
621 hydroxylation reaction to TP-253 is accomplished with the participation of SO_4•$^-$.
622 SO_4•$^-$ is converted to a cation free radical of NEO by plucking an electron from NEO
623 through single electron transfer (SET) and generates hydroxylation product TP-253 by
624 reacting with OH^- in water. Compared to •OH (−1.80 eV), SO_4•$^-$ (−3.43 eV) has the
625 lowest unoccupied molecular orbital energy (E_{LUMO}) and therefore may react with
626 pollutants with a lower activation energy (Fig. 5d) [31]. Similar types of degradation
627 by SET have also been found in oxidative removal processes of various pollutants such
628 as 6-PPD, and anti-degradant used in tire manufacture [66]. Due to the localization
629 effect of the hydroxyl group on the benzene ring, the H in the neighboring hydroxyl
630 group (55H and 56H) becomes a potential site for hydroxylation to TP-269.

631 Second, in Pathway I-2, TP-295 was converted to TP-267 after an amine oxidation
632 reaction driven by •OH at the 12N site. Subsequently, •OH converted TP-267 to TP-
633 283 and TP-299 by successive hydroxylation reactions of the benzene ring. Degradation
634 by amine oxidation following amine hydrolysis has also been reported in previous
635 studies [60]. Interestingly, the yields of TP-283 and TP-299 in the presence of inorganic
636 anions were 10.2 to 35.1-fold higher than those of the system with •OH alone (yields
637 were judged by mass spectral peak Intensity). The above reason is due to the
638 involvement of Cl•, CO_3•$^-$, and NO_2• in the degradation. The E_{LUMO} of Cl• (-4.17 eV),
639 CO_3•$^-$ (-2.46 eV), and NO_2• (-2.24 eV) enables the capture of electrons from NEO by

SET and subsequent hydroxylation. Pathway I-3 was the conversion of the unsaturated double bond in the amide moiety of TP-295 to TP-239 driven by an •OH addition reaction, as well as undergoing phenyl ring hydroxylation to TP-255 and TP-271. Then, pathway I-4 relates to the conversion of TP-295 to TP-235 by decarboxylation of 5C, followed by conversion to TP-205 by again removing the carboxyl group attached to 7C mediated by SO_4•$^-$. Finally, pathway I-5 was similar to I-4 in that it is the product of the decarboxylation of 7C on TP-295. The difference is that the hydroxyl substituent formed after decarboxylation in pathway I-5 was converted to an unsaturated bond in TP-279 by a CO_3•$^-$-mediated hydrolysis reaction rather than to an aldehyde group by direct oxidation.

Pathway II. In pathway II-1 NEO was converted to TP-377 by a •OH-driven HAA reaction (removal of 32H and 35H), and subsequently converted to TP-393 and TP-391 by hydroxylation. NEO can also be directly converted to TP-395, TP-411, and TP-385 *via* consecutive hydroxylation reactions on the benzene ring (path II-2). NEO might also be directly converted to TP-395, TP-411, and TP-385 by three consecutive hydroxylation reactions on the benzene ring (pathway II-2). According to the activity law of carbon atoms, 32H is the most likely site of attack for a third hydroxylation reaction due to its highest reactivity, which is also verified by the abbreviated Fukui function ($f^0 = 0.0231$ and $f^- = 0.0276$). Secondly, 38H and 35H are similarly vulnerable sites for the third hydroxylation reaction (38H: $f^0 = 0.0211$ and $f^- = 0.0318$; 35H: $f^0 = 0.0291$ and $f^- = 0.0177$). The three significantly higher intensity peaks in the EIC of TP-385 also corroborates these conclusions, with retention times of 7.32 min, 8.27 min

662 and 9.03 min, respectively (Fig. S42). Finally, in pathway II-3, an unsaturated bond is
663 formed at 38H by the SO_4•$^-$ driven HAA reaction, in which SO_4•$^-$ synchronized
664 removal of the carboxyl group from the adjacent benzene ring is converted to TP-333.
665 *Pathway III*. Due to the instability of the ester group, NEO was converted to TP-365
666 either spontaneously by an ester hydrolysis reaction or by free radical attack. Similar to
667 the first two pathways, TP-365 can also be converted to TP-381 (presence of Cl• and
668 CO_3•$^-$ driven degradation) and TP-363 by •OH driven hydroxylation and HAA
669 reactions. TP-365 may also be converted to TP-319 by SO_4•$^-$ (or NO_2•) driven
670 decarboxylation and dehydration reactions (pathway III-1). In pathway III-2, the 7C-
671 centered carboxyl group of TP-365 was removed by •OH to produce TP-337 ($f^0 = 0.505$
672 above the other carboxyl group adjacent to the benzene ring). TP-337 was subsequently
673 converted to TP-335 by a direct •OH-driven oxidation reaction hence to TP-170 by an
674 amide hydrolysis reaction to remove the benzene ring. In pathway III-3, based on TP-
675 337, the benzene ring and 32H were attacked by •OH to form the hydroxylation product
676 TP-369 and the unsaturated bond-containing TP-321. Pathway III-4 was found to be
677 initiated entirely by SO_4•$^-$. TP-337 was converted to TP-309 by a second
678 decarboxylation reaction. During subsequent oxidation, TP-309 continues to be
679 converted to hydroxylated TP-341. At the same time, TP-309 was converted to TP-265
680 and TP-281 by a demethylation reaction. Subsequently, a C-N bond break at 12N of
681 TP-265 produced small aliphatic products (TP-114, TP-102 and TP-103).
682

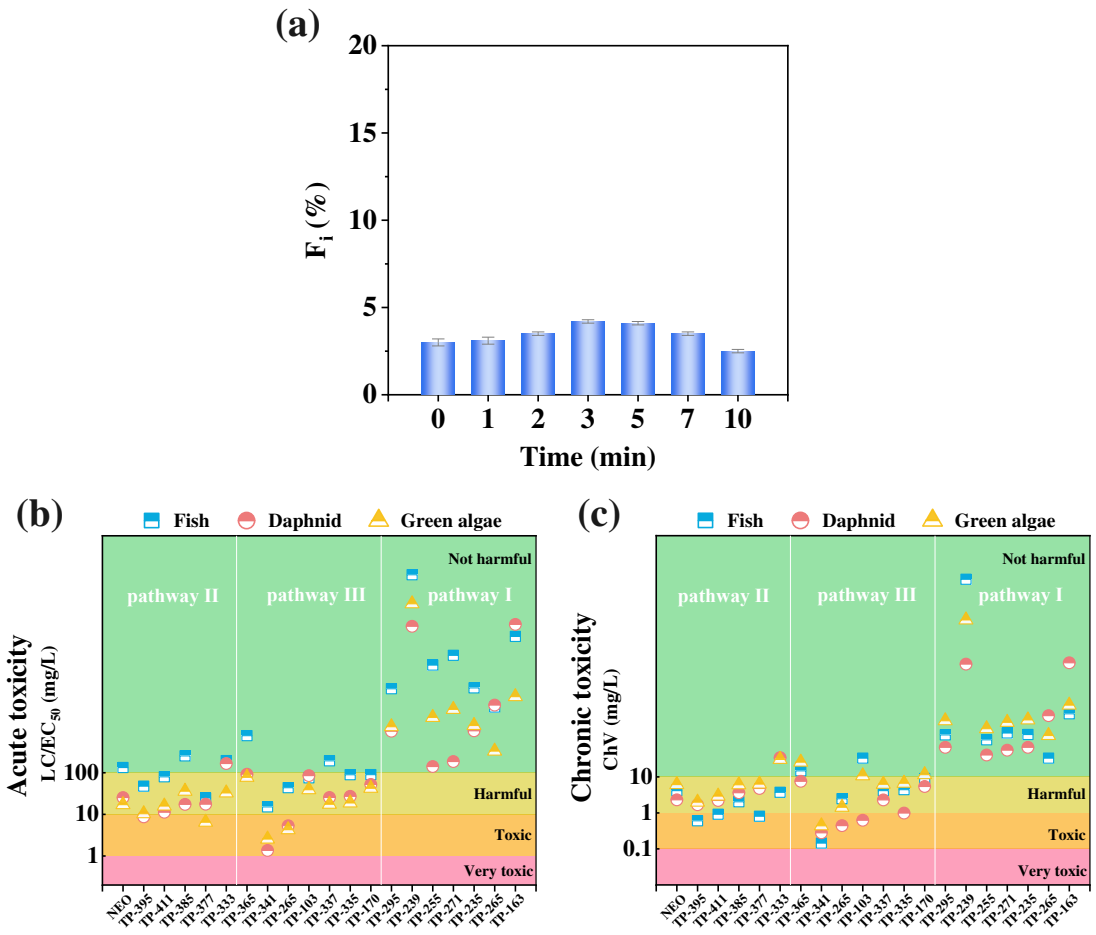

683

684 **Fig. 7.** (a) *Vibrio fischeri* luminescence inhibition rate accompanied by degradation of

685 NEO during UV/PS; (b) acute and (c) chronic toxicity evolution of NEO and its

686 transformation products. Conditions: [PS]= 50 μM, [NEO]= 5 μM, pH=7.

687

688 *3.6. Toxicity evaluation of NEO degradation*

689 The persistence and mobility of TPs in actual waters is often greater than that of their

690 parent compounds which makes them potentially more widespread and enduring in the

691 natural environment, and therefore their toxicity to organisms needs to be understood

692 [42]. Overall solution toxicity (experimental toxicology based on *Vibrio fischeri*) and

693 toxicity of individual TPs (computational toxicology based on ECOSAR software) have

694 been used to comprehensively assess the toxicity levels of TPs during UV/PS

695 experiments. The overall toxicity of the solution was modeled using *Vibrio fischeri* as
696 a model microorganism, and acute toxicity intensity of the samples was expressed in
697 terms of luminescence inhibition (F_i).

698 As shown in Fig. 7a, F_i values of *Vibrio fischeri* showed an increasing and then
699 decreasing trend to 10 min exposure time. Upon completion of the 10 min exposure
700 time the F_i value of *Vibrio fischeri* was 2.5%, achieving partial detoxification compared
701 to the original solution. In addition, the inhibition of *Vibrio fischeri* peaked at 3 min
702 (4.2%), indicating the presence of toxic TPs at the initial stage of degradation. To
703 further characterize toxic TPs in degradation, all TPs of the three degradation pathways
704 were assessed using ECOSAR software (Fig. 7b, 7c and Table S6). The results
705 illustrated that the detoxification effects of the three degradation pathways differed
706 significantly. TPs in Pathway I were significantly less toxic to three aquatic organisms
707 (green algae, fish, and daphnia) than those in Pathways II and III. In Pathway I, acute
708 and chronic toxicity to the three aquatic organisms ranged from "Toxic" or "Harmful"
709 to "Not harmful" when the degradation experiment was completed. As C-N bond
710 breaking is the preferred initiation site for UV/PS degradation of NEO in Pathway I, it
711 is hypothesized that the concentration of TPs in Pathway I is the highest. Therefore,
712 most NEO was removed through pathway I and partial detoxification of the overall
713 toxicity of the solution was achieved. In addition, in Pathways II and III, we found that
714 the toxicity of TPs fluctuated greatly and did not decrease significantly at the end of the
715 reaction. Part of the reason for this phenomenon was the lack of detection of small
716 molecular weight TPs during mass spectrometry. Due to removal of the NEO carboxyl

and nitrogen-containing groups during degradation, the resulting low moleculer weight alkyl compounds were difficult to load with a positive (negative) charge during the MS ionization process and could not be detected. However, it is apparent that the degradation process produces TPs with higher toxicity than the parent NEO. In Pathways II and III, the hydroxylation products (i.e., TP-395 and TP-385), decarboxylation products (TP-337 and TP-309), and aldolization products (i.e., TP-335) formed at an early stage in NEO degradation and reached increased toxicity risk levels of "Toxic" or "Harmful" in terms of the LC/EC_{50} (acute toxicity) and ChV (chronic toxicity) of the three simulated aquatic organisms. Therefore, further attention needs to be paid to the generation and subsequent transformation of toxic TPs, and to monitoring the overall impact on the aquatic environment after NEO release.

4. Conclusion

In this study, the mechanism of NEO degradation and transformation during UV/PS degradation in pure water and actual water matrices was investigated. A kinetic model based on the low concentration probe method is proposed to determine the steady-state concentrations of primary (•OH and SO_4•$^-$) and secondary (Cl•, Cl_2^-•, CO_3•$^-$, and NO_2•) radicals in a variety of systems. In the UV/PS system, the contribution of •OH to NEO degradation increased with increasing alkalinity, but was easily inhibited by NOM. The ranking of k_{obs} for NEO degradation in the presence of inorganic anions was: NO_3^- > pure water ≈ Cl^- > HCO_3^-. In addition, the steady-state concentration of secondary radicals produced by the system was ranked NO_2• > CO_3•$^-$ > Cl_2^-• > Cl•. However,

because of the significant differences in the reactivity of different species of radicals with NEO, the final ranking of the contribution to NEO degradation is: $CO_3^{\bullet -}$ > $NO_2^{\bullet}$ > $Cl^{\bullet}$ > $Cl_2^{\bullet -}$. Based on 39 detected TPs, the oxidation mechanism and the attack of primary and secondary radicals for the degradation of NEO by the UV/PS system were proposed. Toxicity assessment showed that although partial detoxification of NEO was achieved at the end of degradation reaction, the toxicity of hydroxylation products, decarboxylation products, and aldolization products formed at the initial stage of NEO degradation was relatively high.

In addition, some limitations and shortcomings still exist in this study, mainly including (1) the methods to further enhance the degradation rate in actual water still lack in-depth research; (2) the generation of toxic TPs during pollutant degradation cannot be avoided. Future studies should focus on and simulate the degradation of pollutants under actual water in order to further investigate the methods to resist the water matrix effect. Meanwhile, AOPs in practical application need to strictly monitor the formation and toxicity of TPs of the parent pollutants, especially the fate and environmental emissions of highly toxic parts of them in STPs.

Acknowledgements

This work was financially supported by the Key Technology Research and Development Program of Shandong Province (No. 2022CXGC021002-1) and the National Natural Science Foundation of China (Nos. 41977325 and 72074136).

References

[1] Gan, Z., Sun, H., Feng, B., Wang, R., Zhang, Y., 2013. Occurrence of seven artificial sweeteners in the aquatic environment and precipitation of Tianjin, China. Water Res. 47(14), 4928-4937.

[2] Guo, W., Li, J., Liu, Q., Shi, J., Gao, Y., 2021. Tracking the fate of artificial sweeteners within the coastal waters of Shenzhen city, China: from wastewater treatment plants to sea. J. Hazard. Mater. 414, 125498.

[3] World Health Organization, 2023. Aspartame hazard and risk assessment results released. Https://www.who.int/news/item/14-07-2023.

[4] Yang, G., Cao, J., Cui, H., Zhan, X., Duan, G., Zhu, Y., 2023. Artificial sweetener enhances the spread of antibiotic resistance genes during anaerobic digestion. Environ. Sci. Technol. 57(30), 10919-10928.

[5] Chattopadhyay, S., Raychaudhuri, U., Chakraborty, R., 2014. Artificial sweeteners – a review. J. Food Sci. Technol 51(4), 611-621.

[6] Farag, M.A., Rezk, M.M., Hamdi Elashal, M., El-Araby, M., Khalifa, S.A.M., El-Seedi, H.R., 2022. An updated multifaceted overview of sweet proteins and dipeptides as sugar substitutes; the chemistry, health benefits, gut interactions, and safety. Food Res. Int. 162, 111853.

[7] Kumari, A., Arora, S., Choudhary, S., Singh, A.K., Tomar, S.K., 2018. Comparative stability of aspartame and neotame in yoghurt. Int. J. Dairy Technol. 71(1), 81-88.

[8] Subedi, B., Kannan, K., 2014. Fate of artificial sweeteners in wastewater treatment

784 plants in New York State, U.S.A. Environ. Sci. Technol. 48(23), 13668-13674.
785 [9] Anumol, T., Vijayanandan, A., Park, M., Philip, L., Snyder, S.A., 2016.
786 Occurrence and fate of emerging trace organic chemicals in wastewater plants in
787 Chennai, India. Environ. Int. 92-93, 33-42.
788 [10] Gvozdić, E., Bujagić, I.M., Đurkić, T., Grujić, S., 2023. Untreated wastewater
789 impact and environmental risk assessment of artificial sweeteners in river water and
790 sediments of the Danube River Basin in Serbia. Environ. Sci. Pollut. Res 30(35),
791 84583-84594.
792 [11] Li, D., Yao, Y., Sun, H., Wang, Y., Pu, J., Calderón, R., Alder, A.C., Kannan, K.,
793 2020. Artificial sweeteners in pig feed: a worldwide survey and case study in pig
794 farms in Tianjin, China. Environ. Sci. Technol. 54(7), 4059-4067.
795 [12] Shen, G., Lei, S., Li, H., Yu, Q., Wu, G., Shi, Y., Xu, K., Ren, H., Geng, J., 2023.
796 Occurrence and removal of four artificial sweeteners in wastewater treatment plants
797 of China. Environ Sci Proc Imp 25(1), 75-84.
798 [13] Yue, J., Wang, A., Zhao, Y., Zhang, Y., Guo, W., 2024. Distribution and removal
799 characteristics of typical artificial sweeteners in different process stages of sewage
800 treatment plant. J Inner Mongolia Univ Technol (Nat Sci Ed) 43(1), 70-76.
801 [14] Yue, J., Guo, W., Li, D., Zhu, Y., Zhao, Q., Wang, A., Li, J., 2023. Seasonal
802 occurrence, removal and mass loads of artificial sweeteners in the largest water
803 reclamation plant in China. Sci. Total Environ. 856, 159133.
804 [15] Lee, W., Wang, Y., 2015. Assessing developmental toxicity of caffeine and
805 sweeteners in medaka (oryzias latipes). SpringerPlus 4(1).

[16] Chi, L., Bian, X., Gao, B., Tu, P., Lai, Y., Ru, H., Lu, K., 2018. Effects of the artificial sweetener neotame on the gut microbiome and fecal metabolites in mice. Molecules 23(2), 367.

[17] Shil, A., Ladeira Faria, L.M., Walker, C.A., Chichger, H., 2024. The artificial sweetener neotame negatively regulates the intestinal epithelium directly through t1r3-signaling and indirectly through pathogenic changes to model gut bacteria. Front. Nutr. 11, 1366409.

[18] Jiang, L., Yu, Z., Zhao, Y., Yin, D., 2024. Obesogenic potentials of environmental artificial sweeteners with disturbances on both lipid metabolism and neural responses. Sci. Total Environ. 919, 170755.

[19] Yin, R., Zhang, Y., Wang, Y., Zhao, J., Shang, C., 2024. Far-UVC photolysis of peroxydisulfate for micropollutant degradation in water. Environ. Sci. Technol. 58(13), 6030-6038.

[20] Guo, K., Wu, Z., Chen, C., Fang, J., 2022. UV/chlorine process: an efficient advanced oxidation process with multiple radicals and functions in water treatment. Acc. Chem. Res. 55(3), 286-297.

[21] Niu, L., Lin, J., Chen, W., Zhang, Q., Yu, X., Feng, M., 2023. Ferrate(VI)/periodate system: synergistic and rapid oxidation of micropollutants via periodate/iodate-modulated Fe(IV)/Fe(V) intermediates. Environ. Sci. Technol. 57(17), 7051-7062.

[22] Kusic, H., Koprivanac, N., Bozic, A.L., 2006. Minimization of organic pollutant content in aqueous solution by means of AOPs: UV- and ozone-based technologies.

828 Chem. Eng. J. 123(3), 127-137.
829 [23] Yang, J., Zhu, M., Dionysiou, D.D., 2021. What is the role of light in persulfate-
830 based advanced oxidation for water treatment? Water Res. 189, 116627.
831 [24] Lai, F., Tian, F., Xu, B., Ye, W., Gao, Y., Chen, C., Xing, H., Wang, B., Xie, M.,
832 Hu, X., 2022. A comparative study on the degradation of phenylurea herbicides by
833 UV/persulfate process: kinetics, mechanisms, energy demand and toxicity
834 evaluation associated with DBPs. Chem. Eng. J. 428, 132088.
835 [25] Parvizi, T., Parsa, J.B., Farnood, R., 2022. Synergetic photocatalytic fuel cell and
836 CuFe layered doubled hydroxide as photoactivator of persulfate for dramatically
837 electricity generation of organic pollutants degradation. Appl. Catal. B-Environ 319,
838 121894.
839 [26] Kusic, H., Peternel, I., Ukic, S., Koprivanac, N., Bolanca, T., Papic, S., Bozic, A.L.,
840 2011. Modeling of iron activated persulfate oxidation treating reactive azo dye in
841 water matrix. Chem. Eng. J. 172(1), 109-121.
842 [27] Jiang, Z., Wei, J., Niu, X., Cui, X., Li, Y., Cui, N., Li, J., Huo, J., Wang, L., Ji, W.,
843 Li, J., 2024. Highly dispersed Fe_7S_8 anchored on sp^2/sp^3 hybridized carbon boosting
844 peroxymonosulfate activation for enhanced EOCs elimination though singlet
845 oxygen-dominated nonradical pathway. J. Hazard. Mater. 461, 132607.
846 [28] Angkaew, A., Sakulthaew, C., Satapanajaru, T., Poapolathep, A., Chokejaroenrat,
847 C., 2019. UV-activated persulfate oxidation of 17β-estradiol: implications for
848 discharge water remediation. J. Environ. Chem. Eng. 7(2), 102858.
849 [29] Wang, Q., Rao, P., Li, G., Dong, L., Zhang, X., Shao, Y., Gao, N., Chu, W., Xu,

B., An, N., Deng, J., 2020. Degradation of imidacloprid by UV-activated persulfate and peroxymonosulfate processes: kinetics, impact of key factors and degradation pathway. Ecotoxicol. Environ. Saf. 187, 109779.

[30] Liu, X., Liu, Y., Lu, S., Wang, Z., Wang, Y., Zhang, G., Guo, X., Guo, W., Zhang, T., Xi, B., 2020. Degradation difference of ofloxacin and levofloxacin by UV/H_2O_2 and UV/PS (persulfate): efficiency, factors and mechanism. Chem. Eng. J. 385, 123987.

[31] Zhang, H., Xie, C., Chen, L., Duan, J., Li, F., Liu, W., 2023. Different reaction mechanisms of $SO_4^{\bullet-}$ and •OH with organic compound interpreted at molecular orbital level in Co(II)/peroxymonosulfate catalytic activation system. Water Res. 229, 119392.

[32] Lee, M., Wang, W., Du, Y., Hu, H., Huang, N., Xu, Z., Wu, Q., Ye, B., 2020. Enhancement effect among a UV, persulfate, and copper (UV/PS/Cu^{2+}) system on the degradation of nonoxidizing biocide: the kinetics, radical species, and degradation pathway. Chem. Eng. J. 382, 122312.

[33] Cheng, S., Zhao, Y., Pan, Y., Lei, Y., Zhou, Y., Li, C., Zhang, X., Yang, X., 2022. Quantification of the diverse inhibitory effects of dissolved organic matter on transformation of micropollutants in UV/persulfate treatment. Water Res. 223, 118967.

[34] Wang, A., Hua, Z., Chen, C., Wei, W., Huang, B., Hou, S., Li, X., Fang, J., 2021. Radical chemistry and PPCP degradation in the UV/peroxydisulfate process in the presence of chloride at freshwater levels. Chem. Eng. J. 426, 131276.

872 [35] Li, B., Pan, H., Chen, B., 2023. A review of factors affecting the formation and
873 roles of primary and secondary reactive species in UV_{254}-based advanced treatment
874 processes. Water Res. 244, 120537.
875 [36] Wu, Z., Guo, K., Fang, J., Yang, X., Xiao, H., Hou, S., Kong, X., Shang, C., Yang,
876 X., Meng, F., Chen, L., 2017. Factors affecting the roles of reactive species in the
877 degradation of micropollutants by the UV/chlorine process. Water Res. 126, 351-
878 360.
879 [37] Lei, Y., Lu, J., Zhu, M., Xie, J., Peng, S., Zhu, C., 2020. Radical chemistry of
880 diethyl phthalate oxidation via UV/peroxymonosulfate process: roles of primary and
881 secondary radicals. Chem. Eng. J. 379, 122339.
882 [38] Lei, Y., Yu, Y., Lei, X., Liang, X., Cheng, S., Ouyang, G., Yang, X., 2023.
883 Assessing the use of probes and quenchers for understanding the reactive species in
884 advanced oxidation processes. Environ. Sci. Technol. 57(13), 5433-5444.
885 [39] Guo, Y., Long, J., Huang, J., Yu, G., Wang, Y., 2022. Can the commonly used
886 quenching method really evaluate the role of reactive oxygen species in pollutant
887 abatement during catalytic ozonation? Water Res. 215, 118275.
888 [40] Li, J., Zhao, L., Feng, M., Huang, C., Sun, P., 2021. Abiotic transformation and
889 ecotoxicity change of sulfonamide antibiotics in environmental and water treatment
890 processes: a critical review. Water Res. 202, 117463.
891 [41] Rozas, O., Vidal, C., Baeza, C., Jardim, W.F., Rossner, A., Mansilla, H.D., 2016.
892 Organic micropollutants (OMPs) in natural waters: oxidation by UV/H_2O_2 treatment
893 and toxicity assessment. Water Res. 98, 109-118.

894 [42] Zahn, D., Arp, H.P.H., Fenner, K., Georgi, A., Hafner, J., Hale, S.E., Hollender,
895 J., Letzel, T., Schymanski, E.L., Sigmund, G., Reemtsma, T., 2024. Should
896 transformation products change the way we manage chemicals? Environ. Sci.
897 Technol. 58(18), 7710-7718.
898 [43] Li, A.J., Schmitz, O.J., Stephan, S., Lenzen, C., Yue, P.Y., Li, K., Li, H., Leung,
899 K.S., 2016. Photocatalytic transformation of acesulfame: transformation products
900 identification and embryotoxicity study. Water Res. 89, 68-75.
901 [44] Wang, A., Zhu, B., Huang, C., Zhang, W., Wang, M., Li, X., Ling, L., Ma, J., Fang,
902 J., 2023. Generation mechanism of singlet oxygen from the interaction of
903 peroxymonosulfate and chloride in aqueous systems. Water Res. 235, 119904.
904 [45] Chen, C., Wu, Z., Hou, S., Wang, A., Fang, J., 2022. Transformation of
905 gemfibrozil by the interaction of chloride with sulfate radicals: radical chemistry,
906 transient intermediates and pathways. Water Res. 209, 117944.
907 [46] Fu, Y., Li, S., Shi, Y., Geng, J., Li, J., Wu, G., Xu, K., Ren, H., 2019. Removal of
908 artificial sweeteners using UV/persulfate: radical-based degradation kinetic model
909 in wastewater, pathways and toxicity. Water Res. 167, 115102.
910 [47] Hoang, N.T., Nguyen, V.T., Minh Tuan, N.D., Manh, T.D., Le, P., Van Tac, D.,
911 Mwazighe, F.M., 2022. Degradation of dyes by UV/persulfate and comparison with
912 other UV-based advanced oxidation processes: kinetics and role of radicals.
913 Chemosphere 298, 134197.
914 [48] Hong, W., Zou, J., Zhao, M., Yan, S., Song, W., 2024. Development of a five-
915 chemical-probe method to determine multiple radicals simultaneously in hydroxyl

916 and sulfate radical-mediated advanced oxidation processes. Environ. Sci. Technol.
917 58(12), 5616-5626.
918 [49] Yue, J., Guo, W., Zhu, Y., Li, D., Liang, S., Cao, R., Wang, A., Li, J., 2024.
919 Insights on the degradation mechanism of neotame using UV/periodate: Roles of
920 reactive species, kinetics, and pathways. Chem. Eng. J. 495, 153059.
921 [50] Lu, T., Chen, F., 2012. Multiwfn: a multifunctional wavefunction analyzer. J.
922 Comput. Chem. 33(5), 580-592.
923 [51] Ghanbari, F., Yaghoot-Nezhad, A., Wacławek, S., Lin, K.A., Rodríguez-Chueca,
924 J., Mehdipour, F., 2021. Comparative investigation of acetaminophen degradation
925 in aqueous solution by UV/chlorine and UV/H_2O_2 processes: kinetics and toxicity
926 assessment, process feasibility and products identification. Chemosphere 285,
927 131455.
928 [52] Xu, Y., Lin, Z., Wang, Y., Zhang, H., 2017. The UV/peroxymonosulfate process
929 for the mineralization of artificial sweetener sucralose. Chem. Eng. J. 317, 561-569.
930 [53] Mo, C., Tian, F., Xu, B., Lai, F., Gao, Y., Ma, Y., Feng, Z., Yao, Z., Bi, D., Hu,
931 X., 2024. Evaluation and comparison of iohexol elimination by
932 UV/peroxymonosulfate and UV/persulfate processes: radical roles, influence
933 factors and iodinated trihalomethanes formation. J. Water Process. Eng. 67, 106199.
934 [54] Luo, Y., Su, R., Yao, H., Zhang, A., Xiang, S., Huang, L., 2021. Degradation of
935 trimethoprim by sulfate radical-based advanced oxidation processes: kinetics,
936 mechanisms, and effects of natural water matrices. Environ. Sci. Pollut. Res. 28(44),
937 62572-62582.

938 [55] Wang, Z., Shao, Y., Gao, N., Lu, X., An, N., 2018. Degradation of diethyl phthalate
939 (DEP) by UV/persulfate: an experiment and simulation study of contributions by
940 hydroxyl and sulfate radicals. Chemosphere 193, 602-610.
941 [56] Pérez-González, A., Galano, A., 2011. OH radical scavenging activity of
942 edaravone: mechanism and kinetics. J. Phys. Chem. B 115(5), 1306-1314.
943 [57] Lee, M., Wang, W., Xu, Z., Ye, B., Wu, Q., Hu, H., 2019. The application of
944 UV/PS oxidation for removal of a quaternary ammonium compound of dodecyl
945 trimethyl ammonium chloride (DTAC): the kinetics and mechanism. Sci. Total
946 Environ. 655, 1261-1269.
947 [58] Zhou, Y., Chen, C., Guo, K., Wu, Z., Wang, L., Hua, Z., Fang, J., 2020. Kinetics
948 and pathways of the degradation of PPCPs by carbonate radicals in advanced
949 oxidation processes. Water Res. 185, 116231.
950 [59] Lian, L., Yao, B., Hou, S., Fang, J., Yan, S., Song, W., 2017. Kinetic study of
951 hydroxyl and sulfate radical-mediated oxidation of pharmaceuticals in wastewater
952 effluents. Environ. Sci. Technol. 51(5), 2954-2962.
953 [60] Luo, C., Li, M., Cheng, X., Wu, D., Tan, F., Li, Z., Chen, Y., Yu, F., Ma, Q., 2022.
954 Degradation of iopamidol by UV_{365}/NaClO: roles of reactive species, degradation
955 mechanism, and toxicology. Water Res. 222, 118840.
956 [61] Keen, O.S., Love, N.G., Linden, K.G., 2012. The role of effluent nitrate in trace
957 organic chemical oxidation during UV disinfection. Water Res. 46(16), 5224-5234.
958 [62] Ao, X., Zhang, X., Sun, W., Linden, K.G., Payne, E.M., Mao, T., Li, Z., 2024.
959 What is the role of nitrate/nitrite in trace organic contaminants degradation and

transformation during UV-based advanced oxidation processes? Water Res. 253, 121259.

[63] Fu, Y., Wu, G., Geng, J., Li, J., Li, S., Ren, H., 2019. Kinetics and modeling of artificial sweeteners degradation in wastewater by the UV/persulfate process. Water Res. 150, 12-20.

[64] Li, F., Borthwick, A.G.L., Liu, W., 2023. Environmental theoretical calculation for non-periodic systems. Trends Chem. 5(6), 410-414.

[65] Pan, G., Wei, J., Xu, M., Li, J., Wang, L., Li, Y., Cui, N., Li, J., Wang, Z., 2023. Insight into boron-doped biochar as efficient metal-free catalyst for peroxymonosulfate activation: important role of -O-B-O- moieties. J. Hazard. Mater. 445, 130479.

[66] Chen, L., Hu, J., Borthwick, A.G.L., Sun, W., Zhang, H., Jia, D., Liu, W., 2024. Solar-light-activated periodate for degradation and detoxification of highly toxic 6PPD-quinone at environmental levels. Nature Water 2(5), 453-463.